THE JOURNAL OF PHYSICAL CHEMISTRY B
A JOURNAL OF THE AMERICAN CHEMICAL SOCIETY

pubs.acs.org/JPCB

Article

Does Inter-Residue Hydrogen Bonding in β-(1→4)-Linked Disaccharides Influence Linkage Conformation in Aqueous Solution?

Wenhui Zhang, Reagan J. Meredith, Xiaocong Wang, Robert J. Woods, Ian Carmichael, and Anthony S. Serianni*

Cite This: J. Phys. Chem. B 2024, 128, 2317−2325

Read Online

ACCESS | Metrics & More | Article Recommendations | Supporting Information

ABSTRACT: Two disaccharides, methyl β-D-galactopyranosyl-(1→4)-α-D-glucopyranoside (**1**) and methyl β-D-galactopyranosyl-(1→4)-3-deoxy-α-D-*ribo*-hexopyranoside (**3**), were prepared with selective ^{13}C-enrichment to allow measurement of six trans-*O*-glycosidic *J*-couplings ($^{2}J_{COC}$, $^{3}J_{COCH}$, and $^{3}J_{COCC}$) in each compound. Density functional theory (DFT) was used to parameterize Karplus-like equations that relate these *J*-couplings to either ϕ or ψ. *MA'AT* analysis was applied to both linkages to determine mean values of ϕ and ψ in each disaccharide and their associated circular standard deviations (CSDs). Results show that deoxygenation at C3 of **1** has little effect on both the mean values and librational motions of the linkage torsion angles. This finding implies that, if inter-residue hydrogen bonding between O3H and O5′ of **1** is present in aqueous solution and persistent, it plays little if any role in dictating preferred linkage conformation. Hydrogen bonding may lower the energy of the preferred linkage geometry but does not determine it to any appreciable extent. Aqueous 1-μs MD simulation supports this conclusion and also indicates greater conformational flexibility in deoxydisaccharide **3** in terms of sampling several, conformationally distinct, higher-energy conformers in solution. The populations of these latter conformers are low (3−14%) and could not be validated by *MA'AT* analysis. If the MD model is correct, however, C3 deoxygenation does enable conformational sampling over a wider range of ϕ/ψ values, but linkage conformation in the predominant conformer is essentially identical in both **1** and **3**.

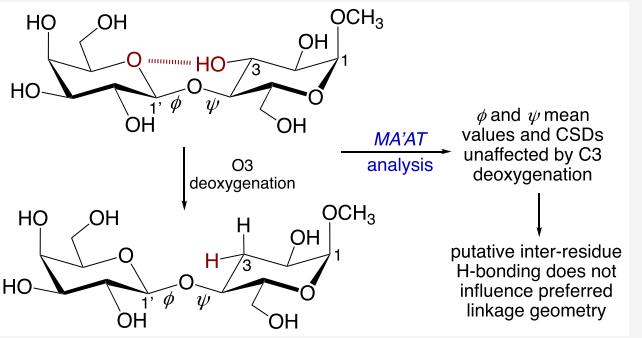

INTRODUCTION

Hydrogen bonding plays an important role in determining the three-dimensional structures and functions of biomolecules, for example, the double helix of DNA and the secondary and tertiary structures of proteins.[1,2] The abundant hydroxyl groups found in saccharides serve as donors and/or acceptors in conventional inter- and intramolecular hydrogen bonding in the solid (crystalline) state and in solution.[3−16] Experimental evidence of hydrogen bonding involving C−H hydrogens as donors has also been reported in aqueous solution.[11,16] In solution, intramolecular hydrogen bonding may play a role in determining the conformations of *O*-glycosidic linkages in oligosaccharides. For example, hydrogen bonding between O3H and O5′ is commonly observed in the crystal structures of disaccharides containing β-(1→4) linkages wherein O3 of the acceptor residue is equatorial and both residues adopt $^{4}C_{1}$ chair conformations with D-configurations, which pertains to methyl α-lactoside (methyl β-D-galactopyranosyl-(1→4)-α-D-glucopyranoside) (**1**) and methyl β-lactoside (methyl β-D-galactopyranosyl-(1→4)-β-D-glucopyranoside) (**2**) (Scheme 1).[17,18] In crystal structures of **1** and **2**, differences of 6−15° are observed for ϕ (C′−C1′−O4−C4 torsion angle) and ψ (C1′−O4−C4−C3 torsion angle) in their *O*-glycosidic linkages (ϕ = 148.1° and ψ = 93.5° in **1**; ϕ = 153.9° and ψ = 78.3° in **2**). An inspection of crystal structure parameters (Table 1) shows that internuclear distances between O3 and O5′ are 2.824 and 2.764 Å in **1** and **2**, respectively, consistent with hydrogen bonding. Hydrogen bond linearity is greater in **1** than in **2**, and pseudo torsion angles C2′−C1′−O5′···O3H and C4−C3−O3−H suggest localized electron density on O5′ (sp^3-like lone-pair orbitals). Recent NMR studies using *MA'AT* analysis[19,20] have shown that, in aqueous solution, linkage conformations of **1** and **2** are very similar (ϕ = 28° and ψ = −8° in **1**; ϕ = 29° and ψ = −8° in **2**).[21] These geometries are compatible with inter-residue hydrogen bonding between O5′ and O3H, given the O5′−O3 internuclear distances.

Received: November 10, 2023
Revised: January 26, 2024
Accepted: February 2, 2024
Published: February 28, 2024

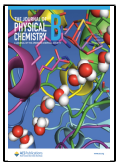

https://doi.org/10.1021/acs.jpcb.3c07448
J. Phys. Chem. B 2024, 128, 2317−2325

Scheme 1. Structures of Disaccharides 1 and 2 Showing Atom Numbering and Putative Inter-Residue Hydrogen Bonding (in Red) between O3H (Donor) and O5′ (Acceptor)

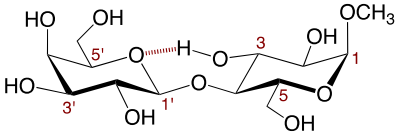

methyl α-lactoside (**1**)
methyl β-D-galactopyranosyl-(1→4)-α-D-glucopyranoside

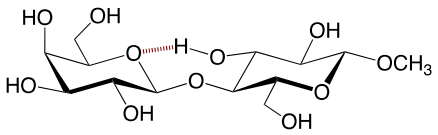

methyl β-lactoside (**2**)
methyl β-D-galactopyranosyl-(1→4)-β-D-glucopyranoside

Scheme 2. Redundant *J*-Couplings across the *β*-(1→4) *O*-Glycosidic Linkage in 3[a]

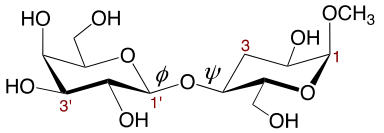

methyl β-D-galactopyranosyl-(1→4)-3-deoxy-α-D-*ribo*-hexopyranoside (**3**)

ϕ		ψ	
$^2J_{C1',C4}$		$^3J_{C1',H4}$	$^2J_{C3,H4}$
$^3J_{H1',C4}$		$^3J_{C1',C3}$	$^2J_{C5,H4}$
$^3J_{C2',C4}$		$^3J_{C1',C5}$	$^2J_{C3,C5}$
$^2J_{C2',H1'}$			

[a]Values shown in red are conventional constraints, and those shown in black are unconventional constraints, used in *MA′AT* analysis. The values in red were used in this study. See Scheme 3 and the text for details.

The observation of inter-residue hydrogen bonding in **1** and **2** in the crystalline state and the compatibility of linkage conformation with this hydrogen bonding in aqueous solution raise the question of whether inter-residue hydrogen bonding plays an active role in dictating preferred linkage conformation in **1** and **2**, or is a fortuitous (secondary) consequence of preferred linkage geometry dictated by other dominant structural factors (e.g., stereoelectronic[22−27] and steric effects, solvation). To answer this question, disaccharide **1** was prepared in which O3 of the *α*Glc residue was replaced with hydrogen to give the C3-deoxy derivative, methyl *β*-D-galactopyranosyl-(1→4) 3-deoxy-*α*-D-*ribo*-hexopyranoside (**3**) (Scheme 2). Disaccharide **3** was prepared with single ^{13}C-labeling at C1′ and C2′ to enable measurements of redundant NMR spin-couplings, $^3J_{COCH}$, $^2J_{COC}$, and $^3J_{COCC}$, across its internal *O*-glycosidic linkage (Scheme 2).[28−31] *MA′AT* analysis was then applied to these *J*-couplings in **3** to obtain mean values of the *ϕ* and *ψ* that comprise its linkage (Scheme 2) and their circular standard deviations (CSDs) to gain insight into their librational averaging. The advantage of *MA′AT* analysis for this comparison is the ability of the method to provide experiment-based probability distributions of molecular torsion angles in solution and to give mean angles with high precision and accuracy.[19−21] Evidence of significant differences in the linkage conformations in **1** and **3** would support the argument that inter-residue hydrogen bonding plays a role in dictating preferred linkage conformation in aqueous solution, whereas identical (or near identical) conformations would suggest that this hydrogen bonding, if persistent in solution, is not a major determinant of linkage conformation. The results of these studies are described in this report.

METHODS

Experimental Section. *Preparation of ^{13}C-Labeled Disaccharide 3.* ^{13}C-Labeled disaccharides $\mathbf{3}^{1'}$ and $\mathbf{3}^{2'}$ (the superscripts denote the ^{13}C-labeled carbons in **3**) were prepared from D-[1-^{13}C]galactose and D-[2-^{13}C]galactose, respectively. Descriptions of the chemical syntheses of $\mathbf{3}^{1'}$ and $\mathbf{3}^{2'}$ are found in the Supporting Information. D-[1-^{13}C]-galactose and D-[2-^{13}C]galactose were prepared by established methods.[32,33]

NMR Spectroscopy. High-resolution 1D ^{1}H and ^{13}C{^{1}H} NMR spectra were obtained using 5-mm NMR tubes on a 600-MHz FT-NMR spectrometer equipped with a 5-mm ^{1}H−^{19}F/^{15}N−^{31}P AutoX dual broadband probe. NMR spectra of synthetic intermediates were collected in $CDCl_3$ at 22 °C. ^{1}H NMR spectra (600 MHz) were collected with a ∼6000 Hz spectral window and an ∼4.0 s recycle time, and ^{13}C{^{1}H} NMR spectra (150 MHz) were collected with an ∼30,000 Hz spectral window and ∼3.0 s recycle time. ^{1}H and ^{13}C Chemical shifts were referenced internally to the residual $CHCl_3$ signal in the $CDCl_3$ solvent.

High-resolution ^{1}H and ^{13}C{^{1}H} NMR spectra of **3**, $\mathbf{3}^{1'}$, and $\mathbf{3}^{2'}$ were obtained on ∼20 and ∼100 m*M* aqueous (^2H_2O) solutions, respectively, at 22 °C. ^{1}H NMR spectra were collected with a ∼2800 Hz spectral window and ∼4 s recycle time, and FIDs were zero-filled to give final digital resolutions of <0.01 Hz/pt. ^{13}C{^{1}H} NMR spectra were collected with a ∼12,800 Hz spectral window and ∼5 s recycle time, and FIDs were zero-filled to give final digital resolutions of <0.05 Hz/pt. FIDs were processed with resolution enhancement (Gaussian or sine-bell functions) to improve resolution and facilitate the measurement of small *J*-couplings (≥0.5 Hz), and reported *J*-

Table 1. Internuclear Distances, Pseudo Bond Angles, and Pseudo Torsion Angles[a] Relevant to Inter-Residue Hydrogen Bonding between O3H and O5′ in Crystal Structures of 1 and 2

cmpd	internuclear distances (Å)				pseudo bond angles (°)		pseudo torsion angles (°)	
	O5′···O3	O5′···O3H	O3−O3H	|Δ| (Å)[b]	C1′−O5′···O3H	O5′···H−O3	C2′−C1′−O5′···O3H	C4−C3−O3−H
1	2.824	2.061	0.840	0.077	101.5	150.8	172.2	60.5
2	2.764	2.079	0.819	0.134	101.7	140.9	−176.0	78.0

[a]All values were extracted from the X-ray crystal structures of **1** (ref 17) and **2** (ref 18). [b]$|\Delta| = |[O'_a\cdots H_d + O_d - H_d] - [O'_a\cdots O_d]|$. As this difference approaches zero, the hydrogen bond approaches linearity.

https://doi.org/10.1021/acs.jpcb.3c07448
J. Phys. Chem. B 2024, 128, 2317−2325

couplings are accurate to ±0.1 Hz unless otherwise stated (representative 1D ^{1}H and ^{13}C{^{1}H} NMR spectra of **3** are shown in Figures S1−S3 in the Supporting Information). $^{3}J_{C1',H4}$ and $^{3}J_{C4,H1'}$ values in **3** were measured at natural abundance from 2D ^{13}C−^{1}H *J*-HMBC spectra,[34] which were obtained with a 2-fold low-pass *J*-filter to suppress $^{1}J_{CH}$ values (Figures S4 and S5, Supporting Information). J-HMBC spectra were recorded with spectral widths of 4.2 ppm in the ^{1}H dimension and 90.0 ppm in the ^{13}C dimension, 24 scans per t_1 increment, and initial matrices of 2048 and 256 data points in the ^{1}H and ^{13}C dimensions, respectively. Prior to Fourier transformation, zero-filling was performed to give final 8192 × 1024 matrices in the ^{1}H and ^{13}C dimensions, respectively, which were multiplied by squared cosine-bell window functions during processing. A 2-fold low-pass J-filter (τ_1 = 2.50 ms and τ_2 = 1.66 ms) was applied to suppress $^{1}J_{CH}$ correlations. A long coupling evolution delay (Δ) of 500 ms was used to allow large scaling factors (κ) of 47 and 71 to be applied in the indirect dimension.

Computational Section. *Geometric Optimization of Model Disaccharide* ***3*****^{c}**. Density functional theory (DFT) calculations were conducted on model disaccharide **3**^{c} (the superscript "c" denotes an *in silico* structure of **3**) with *Gaussian*09[35] using the B3LYP functional[36] and 6-31G* basis set[37] for geometry optimization. The effects of solvent water were treated using the self-consistent reaction field (SCRF)[38] and the integral equation formalism (polarizable continuum) model (IEFPCM).[39] Exocyclic C−C and C−O torsion angles in **3**^{c} were constrained as summarized in Scheme S2 (Supporting Information), and only one set of these angles was investigated at each incremented value of the *O*-glycosidic torsion angles, *phi* (ϕ) and *psi* (ψ), torsion angles ϕ (defined as H1′−C1′−O4−C4) and ψ (defined as C1′−O4−C4−H4) were varied in 15° increments through 360° and held constant during geometry optimization, giving 576 geometry-optimized structures.

Calculations of NMR Spin-Coupling Constants in ***3*****^{c}**. J_{HH}, J_{CH}, and J_{CC} values were calculated in each geometry-optimized structure of **3**^{c} using DFT and the B3LYP functional[36] in *Gaussian*09.[35] The Fermi contact,[40−42] diamagnetic and paramagnetic spin−orbit, and spin-dipole terms[40] were recovered using a specially designed basis set, [5s2p1d|3s1p],[43] and raw (unscaled) calculated *J*-couplings are reported and are accurate to within ±0.2−0.3 Hz based on prior work.[43] The self-consistent reaction field (SCRF)[38] and the integral equation formalism (polarizable continuum) model (IEFPCM)[39] were used to treat the effects of solvent water during the *J*-coupling calculations. Three *J*-couplings were used to model ϕ and three *J*-couplings were used to model ψ in **3** (Scheme 2). Equations relating the six *J*-couplings to either ϕ or ψ were parameterized using the scipy and numpy packages in *Python* and a subpopulation of conformers that was selected using an energy cutoff to remove sterically strained conformers.[21,44] The goodness-of-fit of each equation is reported as a root mean squared deviation (rmsd).

Determination of Linkage Conformation in ***3*** *Using J-Coupling Ensembles and MA′AT Analysis.* Experimental NMR *J*-couplings (three values each for ϕ and ψ; Schemes 2 and 3) and DFT-parameterized equations for each *J*-coupling were combined with Fredholm theory and circular statistics to determine conformational populations of the β-(1→4) linkage in **3**, using the statistical software, *MA′AT*.[19,20] The current version of *MA′AT*, and a User Manual, can be accessed online at: https://rmeredit.shinyapps.io/maat24/. Linkage torsion angles, ϕ and ψ, were modeled as wrapped Gaussian distributions to give the mean and circular standard deviation (CSD) of each angle.

Scheme 3. Structures of 3 and Its ^{13}C Isotopomers 3$^{1'}$ and 3$^{2'}$ from Which the ϕ- and ψ-Dependent trans-Glycosidic *J*-Values Shown on the Right Were Obtained[a]**

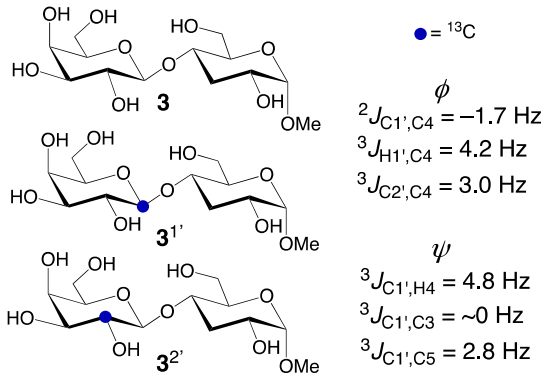

[a]See text for the definitions of the superscripts.

Aqueous Molecular Dynamics Simulations of ***1*****^{c}** *and* ***3*****^{c}**. Initial structures of **1**^{c} and **3**^{c} were built using the carbohydrate builder module available at the GLYCAM Web site (http://www.glycam.org).[45] The GLYCAM06[46] (version j) force field was employed in all simulations. Structures **1**^{c} and **3**^{c} were solvated with TIP3P[47] water using a 12 Å buffer in a cubic box, using the LEaP module in the AMBER14 software package.[48] Energy minimizations for solvated **1**^{c} and **3**^{c} were performed separately under constant volume (500 steps steepest descent, followed by 24,500 steps of conjugate-gradient minimization). Each system was subsequently heated to 300 K over a period of 50 ps, followed by equilibration at 300 K for a further 0.5 ns using the nPT condition, with the Berendsen thermostat[49] for temperature control. All covalent bonds involving hydrogen atoms were constrained using the SHAKE algorithm,[50] allowing a simulation time step of 2 fs throughout the simulation. After equilibration, production simulations were carried out with the GPU implementation[51] of the PMEMD.MPI module, and trajectory frames were collected every 1 ps for a total of 1 μs. One to four nonbonded interactions were not scaled,[52] and a nonbonded cutoff of 8 Å was applied to van der Waals interactions, with long-range electrostatics treated with the particle mesh Ewald approximation. The output of each MD simulation was imported into *Prism*[53] for visualization.

RESULTS AND DISCUSSION

Three-Bond ^{13}C−^{1}H Spin-Coupling Constants. Trans-glycosidic vicinal $^{3}J_{COCH}$ values in **1**^{c} and **3**^{c} exhibit dynamic ranges of ~10 Hz, as shown in Figure 1 and in 2D contour plots (Figures S6 and S7, Supporting Information). The ϕ-dependent $^{3}J_{C4,H1'}$ values are essentially unaffected by ψ and the ψ-dependent $^{3}J_{C1',H4}$ values are essentially unaffected by ϕ (i.e., both exhibit minimal secondary effects). $^{3}J_{COCH}$ values in **1** and **3** show very similar dependencies on the C−O−C−H torsion angle and give very similar parameterized equations (eqs S1, S2, S7, and S8), demonstrating that deoxygenation at C3 of the Glc residue does not affect the behaviors of these trans-glycosidic $^{3}J_{COCH}$ values. Given the high degree of similarity of eqs S1, S2, S7, and S8, the total data set was

https://doi.org/10.1021/acs.jpcb.3c07448
J. Phys. Chem. B 2024, 128, 2317−2325

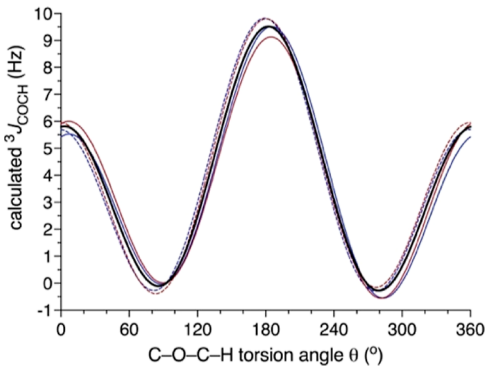

Figure 1. Plots of calculated trans-glycosidic $^3J_{COCH}$ values in **1** and **3** as a function of θ, where θ can be either ϕ (for $^3J_{H1',C4}$) or ψ (for $^3J_{C1',H4}$). Solid red curve, $^3J_{H1',C4}$ in **3** (eq S2). Dashed red curve, $^3J_{C1',H4}$ in **3** (eq S8). Solid blue curve, $^3J_{H1',C4}$ in **1** (eq S1). Dashed blue curve, $^3J_{C1',H4}$ in **1** (eq S7). Solid black curve, generalized curve obtained from averaging the four data sets (eq 1).

combined to give a generalized parameterized equation, eq 1, in which θ is the C−O−C−H torsion angle. Equation 1 was used in *MA'AT* analyses of the linkages in $\mathbf{1}^c$ and $\mathbf{3}^c$.

$$^3J_{COCH}\ (\text{Hz}) = 3.79 - 1.85\cos\theta + 3.86\cos 2\theta + 0.36\sin 2\theta \qquad \text{rmsd} = 0.70\ \text{Hz} \tag{1}$$

Two-Bond $^{13}C-^{13}C$ Spin-Coupling Constants. Trans-glycosidic geminal $^2J_{COC}$ values in $\mathbf{1}^c$ and $\mathbf{3}^c$ have dynamic ranges of ∼4.5 Hz, as shown in Figure 2 and in 2D contour

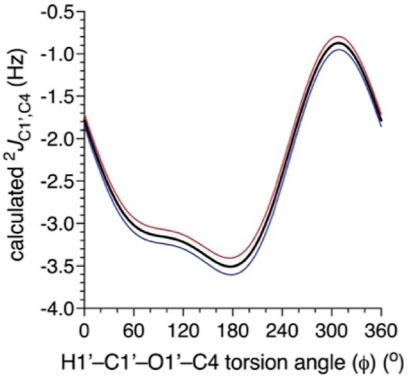

Figure 2. Plots of DFT-calculated $^2J_{C1',C4}$ values in $\mathbf{1}^c$ and $\mathbf{3}^c$ as a function of ϕ. Red curve, $\mathbf{3}^c$ (eq S4). Blue curve, $\mathbf{1}^c$ (eq S3). Black curve, generalized curve described by eq 2 obtained by averaging eqs S3 and S4.

plots (Figure S6, Supporting Information). These *J*-values depend primarily on ϕ, but there is a significant secondary dependence on ψ.[30,54,55] They are uniformly negative in sign, with the most negative values associated with H1′−C1′−O1′−C4 torsion angles near 180° and the least negative near −60°. $^2J_{COC}$ values in $\mathbf{1}^c$ and $\mathbf{3}^c$ show similar dependencies on ϕ (Figure 2) and consequently give similar parameterized equations (eqs S3 and S4, Supporting Information). As found for the trans-glycosidic $^3J_{COCH}$ values, $^2J_{COC}$ values are unaffected by deoxygenation at C3 of the Glc residue. Given the similarity of eqs S3 and S4, the total data set was combined to give a generalized parameterized equation, eq 2, which was used in *MA'AT* analyses of the linkages in **1** and **3**.

$$^2J_{C1',C4}\ (\text{Hz})(\text{gen}) = -2.48 + 0.86\cos\phi - 0.84\sin\phi - 0.17\cos 2\phi - 0.38\sin 2\phi \qquad \text{rmsd} = 0.40\ \text{Hz} \tag{2}$$

Three-Bond $^{13}C-^{13}C$ Spin-Coupling Constants. $^3J_{C1',C3}$. The trans-glycosidic C−O−C−C coupling pathway most likely to be affected by deoxygenation at C3 of **1** is that associated with $^3J_{C1',C3}$. Plots of calculated $^3J_{C1',C3}$ values as a function of ψ in $\mathbf{1}^c$ and $\mathbf{3}^c$ are shown in Figure 3A. The two curves have

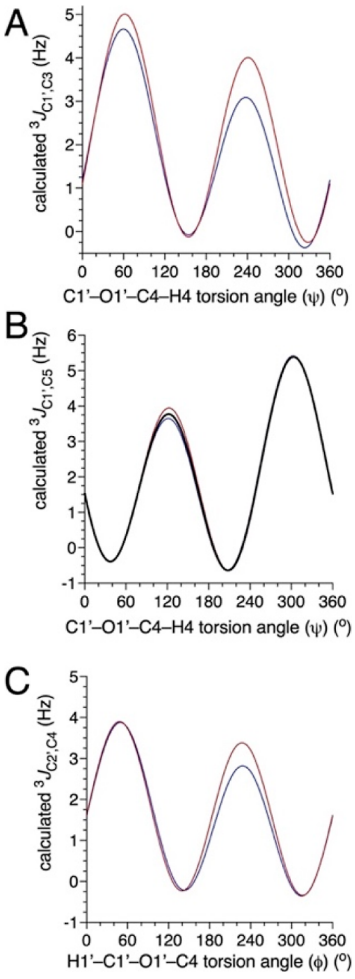

Figure 3. Plots of DFT-calculated $^3J_{COCC}$ values in $\mathbf{1}^c$ and $\mathbf{3}^c$. Red curves, $\mathbf{3}^c$. Blue curves, $\mathbf{1}^c$. (A) $^3J_{C1',C3}$ as a function of ψ (eqs 3 and 4). (B) $^3J_{C1',C5}$ as a function of ψ (eqs S11 and S12). Black curve, generalized curve (eq 5) obtained from averaging the two curves for $\mathbf{1}^c$ and $\mathbf{3}^c$. (C) $^3J_{C2',C4}$ as a function of ϕ (eqs S5 and S6).

identical phases but different amplitudes, with that for $\mathbf{3}^c$ (deoxy) greater than that for $\mathbf{1}^c$ (oxy). The different amplitudes are caused mainly by distinctly different *J*-values at ψ = 60 and 240°, which correspond to C1′−O1′−C4−C3 torsion angles of 180 and 0°, respectively. The data indicate that the addition of an hydroxyl group to the terminal coupled carbon bonded to carbon either has little or no effect on the $^3J_{C1',C3}$ or reduces its magnitude depending on the torsion angle subtended by the coupled carbons. Whether the same effect occurs at the coupled carbon bonded to oxygen could not be determined. The effect of C3−O3 bond conformation on calculated $^3J_{C1',C3}$ values in **1** was also not investigated and may affect the difference between calculated $^3J_{C1',C3}$ values in $\mathbf{1}^c$

https://doi.org/10.1021/acs.jpcb.3c07448
J. Phys. Chem. B 2024, 128, 2317−2325

and $\mathbf{3}^c$. Terminal in-plane contributions to $^3J_{COCC}$,[28] which could affect the difference between $^3J_{C1',C3}$ in $\mathbf{1}^c$ and $\mathbf{3}^c$, are not possible for $^3J_{C1',C3}$ in $\mathbf{1}^c$ since O3 can never lie in the coupling plane due to structural constraints imposed by the pyranosyl ring (Scheme 4). Nevertheless, the two curves for $\mathbf{1}^c$ and $\mathbf{3}^c$ in

Scheme 4. C1′−O1′−C4−C3 Coupling Pathway in 1 Relevant to $^3J_{C1',C3}$ (Highlighted in Red)[a]

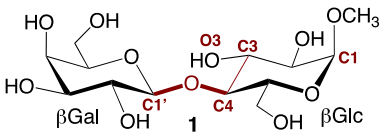

[a]The C1′−O1′−C4−C3 and O1′−C4−C3−O3 torsion angles must be ∼180° for O3 to lie in the coupling plane. The latter torsion angle is not achievable due to the highly preferred $^4C_1$ chair form of the βGlc ring. An "in-plane" O3 is achievable when the βGlc ring adopts the $^4C_1$ chair form, but the latter is minimally populated in solution.

Figure 3A were judged to be sufficiently different to require the use of specific eqs 3 and 4 to treat ψ in **1** and **3**, respectively, by *MA′AT* analysis.

$$^3J_{C1',C3}\ (\mathrm{Hz})(\mathbf{1}^c) = 1.84 + 0.28\cos\psi + 0.75\sin\psi - 0.94\cos 2\psi + 1.80\sin 2\psi \qquad \mathrm{rmsd} = 0.46\ \mathrm{Hz} \tag{3}$$

$$^3J_{C1',C3}\ (\mathrm{Hz})(\mathbf{3}^c) = 2.17 + 0.18\cos\psi + 0.47\sin\psi - 1.26\cos 2\psi + 1.97\sin 2\psi \qquad \mathrm{rmsd} = 0.78\ \mathrm{Hz} \tag{4}$$

$^3J_{C1',C5}$. The plots of DFT-calculated $^3J_{C1',C5}$ values in $\mathbf{1}^c$ and $\mathbf{3}^c$ as a function of ψ highly overlap, with minor differences observed at $\psi = 120°$, corresponding to a C1′−O1′−C4−C5 torsion angle of 0° (eclipsed geometry) (Figure 3B). Given the similarity of the two parameterized equations (eqs S11 and S12, Supporting Information), generalized eq 5, obtained by averaging eqs S11 and S12, was used to treat ψ in *MA′AT* analyses of **1** and **3**.

$$^3J_{C1',C5}\ (\mathrm{Hz})(\mathrm{gen}) = 2.05 + 0.54\cos\psi - 0.61\sin\psi - 1.06\cos 2\psi - 2.30\sin 2\psi \qquad \mathrm{rmsd} = 0.66\ \mathrm{Hz} \tag{5}$$

$^3J_{C2',C4}$. The plots of DFT-calculated $^3J_{C2',C4}$ values in $\mathbf{1}^c$ and $\mathbf{3}^c$ as a function of ϕ highly overlap at ϕ values of 0−120°, but differ significantly at values between 120−300°, with $\mathbf{3}^c$ giving slightly larger couplings than $\mathbf{1}^c$ (Figure 3C). At $\phi = 240°$, where the difference is greatest, the C2′−C1′−O1′−C4 torsion angle is 0° (eclipsed geometry). The two curves were judged to be sufficiently different to require the use of specific eqs 6 and 7 to treat ϕ in $\mathbf{1}^c$ and $\mathbf{3}^c$, respectively, by *MA′AT* analysis.

$$^3J_{C2',C4}\ (\mathrm{Hz})(\mathbf{1}^c) = 1.54 + 0.29\cos\phi + 0.45\sin\phi - 0.25\cos 2\phi + 1.79\sin 2\phi \qquad \mathrm{rmsd} = 0.37\ \mathrm{Hz} \tag{6}$$

$$^3J_{C2',C4}\ (\mathrm{Hz})(\mathbf{3}^c) = 1.68 + 0.13\cos\phi + 0.23\sin\phi - 0.20\cos 2\phi + 1.95\sin 2\phi \qquad \mathrm{rmsd} = 0.34\ \mathrm{Hz} \tag{7}$$

Hypersurfaces showing the effects of ϕ and ψ rotation on DFT-calculated trans-*O*-glycosidic *J*-couplings in $\mathbf{1}^c$ and $\mathbf{3}^c$ are shown in Figures S6 and S7 (Supporting Information). The colored curves in Figures 1−3 were derived from DFT-calculated *J*-values in $\mathbf{1}^c$ and $\mathbf{3}^c$ as a function of rotating both ϕ and ψ through 360° (see Computational Section). The full DFT data for $\mathbf{3}^c$ are given in Figure S8 (Supporting Information), which shows the degree of *y*-axis scatter caused by rotating one of these angles through 360° while holding the other angle constant. All data points were used to obtain a parameterized equation for the given *J*-coupling.

D. *MA′AT* Analyses of ϕ and ψ in 1 and 3. Parameterized *J*-coupling equations and experimental trans-*O*-glycosidic *J*-couplings (Table 2) were used to model ϕ and

Table 2. Experimental Trans-*O*-glycosidic $^{13}C-^1H$ and $^{13}C-^{13}C$ Spin-Coupling Constants[a] in 1 and 3

compd	ϕ-dependent *J*-couplings			ψ-dependent *J*-couplings		
	$^2J_{C1',C4}$	$^3J_{C4,H1'}$	$^3J_{C2',C4}$	$^3J_{C1',H4}$	$^3J_{C1',C3}$	$^3J_{C1',C5}$
1	−2.0	3.9	3.1	5.1	*br*	2.0
3	−1.7	4.2	3.0	4.8	∼0	2.8

[a]In Hz ± 0.1 Hz; 22 °C in ^2H_2O; *br* denotes broadened signal (J < 0.5 Hz). The *J*-couplings for **1** were taken from reference;[21] the *J*-couplings for **3** were obtained in this work.

ψ in **1** and **3** using *MA′AT* analysis (Figure 4). The mean torsion angles, circular standard deviations (CSDs) of these angles, and rmsds obtained from these analyses are shown in Table 3.

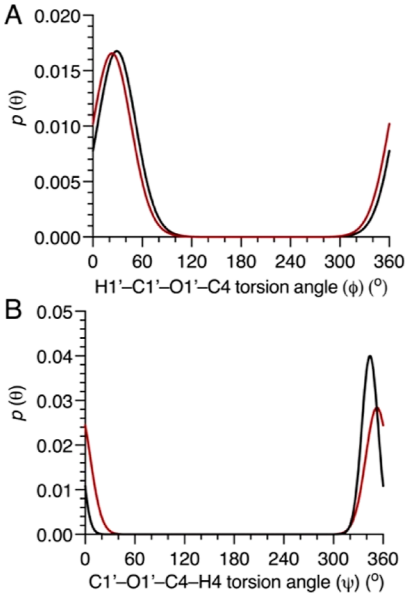

Figure 4. Probability distributions of ϕ (A) and ψ (B) determined from single-state *MA′AT* modeling of the *O*-glycosidic linkages in **1** (black curves) and **3** (red curves).

The conformational properties of the β-(1→4) linkages in **1** and **3** are similar but not identical. The mean value of ϕ in **1** is ∼29° in **1** and ∼23° in **3**, giving a ∼ 6° difference. The CSDs of both angles (∼26 and 24°) are similar, indicating similar librational averaging about the mean angles. Rmsds calculated from single-state *MA′AT* models are 0.3−0.4 Hz, indicative of good fits to the experimental *J*-couplings. Parameter space

https://doi.org/10.1021/acs.jpcb.3c07448
J. Phys. Chem. B 2024, 128, 2317−2325

Table 3. Statistical Parameters Obtained from Single-State *MA'AT* Modeling of ϕ and ψ in 1 and 3

compd	*phi* (ϕ)			*psi* (ψ)		
	mean ± SE[a] (°)	CSD[b] ± SE (°)	rmsd[c] (Hz)	mean ± SE (°)	CSD ± SE (°)	rmsd (Hz)
1	28.9 ± 9.8	26.2 ± 14.1	0.28	−7.5 ± 6.3	13.8 ± 13.8	0.24
3	23.1 ± 10.6	24.4 ± 12.4	0.39	−15.9 ± 5.9	9.9 ± 18.3	0.21

[a]SE = standard error. [b]CSD = circular standard deviation. [c]rmsd = root mean squared deviation.

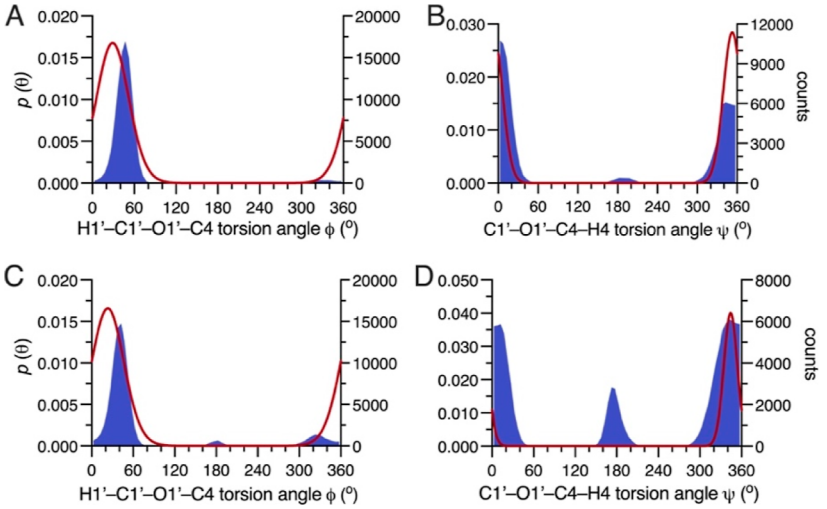

Figure 5. Histograms (filled blue) showing the distributions of ϕ and ψ obtained from aqueous MD simulations of **1**[c] (A,B) and **3**[c] (C,D), superimposed on *MA'AT* models of these angles (red curves).

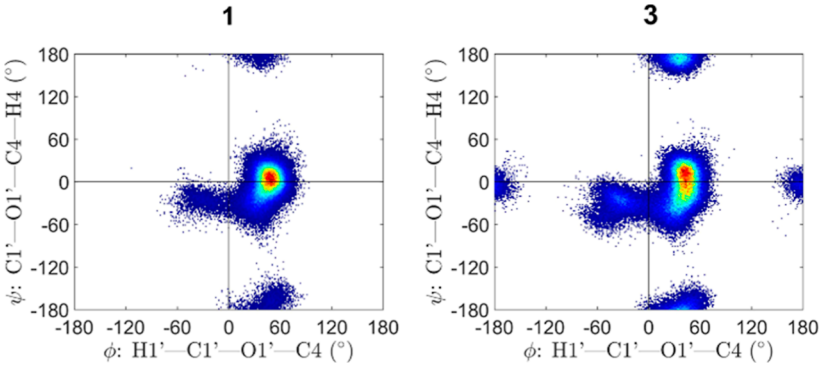

Figure 6. ϕ/ψ plots obtained from 1-μs aqueous MD simulations of **1**[c] (left) and **3**[c] (right) showing enhanced conformational space accessible to **3**[c] relative to **1**[c].

plots for ϕ and ψ in **1** and **3** show unique fits of the experimental *J*-couplings to single-state models, especially for ψ (Figure S9, Supporting Information). The mean values of ψ in **1** and **3** differ slightly, adopting values of ∼−8° in **1** and ∼−16° in **3**, giving a ∼8° difference. The CSDs calculated for both angles are similar (10−14°) and are smaller than those found for ϕ. Rmsds calculated for single-state analyses of ψ are 0.21−0.24 Hz, again showing very good fits to the experimental *J*-values. These results show that deoxygenation at C3 of the Glc residue in **1** causes only minor changes in both ϕ and ψ, implying that inter-residue hydrogen bonding between the two residues that may exist in aqueous solution exerts only minor effects on preferred linkage geometry, that is, linkage conformation is largely dictated by other noncovalent factors. If hydrogen bonding between O3H and O5′ in **1** is persistent in aqueous solution, it likely results in a lowering of the conformational energy of the molecule (it stabilizes the linkage but does not dictate it).

Potential Energy Surfaces for, and MD Simulations of, 1[c] and 3[c]. The most stable linkage conformers of **1**[c] and **3**[c] determined from DFT-determined potential energy surfaces (PESs) (Figure S10, Supporting Information) contain essentially identical values of ϕ (∼161° when ϕ is defined as C2′−C1′−O1′−C4), whereas ψ values differ significantly (130° in **1**[c] and 98° in **3**[c], when ψ is defined as C1′−O1′−C4−C3). These angles translate into ∼40° for ϕ = H1′−C1′−O1′−C4, and values of 10 and −22° for **1**[c] and **3**[c], respectively, when ψ = C1′−O1′−C4−H4. The maps, however, were derived from a limited inspection of the conformational space available to **1**[c] and **3**[c], and consequently, preferred values of ϕ and ψ predicted from them are not very reliable. Nevertheless, the differences between *MA'AT*- and PES-derived ϕ and ψ values in the preferred linkage conformations of **1** and **3** are modest, with PES giving ϕ values that differ by 10−20° from those obtained from *MA'AT* analysis, and PES showing the

https://doi.org/10.1021/acs.jpcb.3c07448
J. Phys. Chem. B 2024, 128, 2317−2325

correct trend in ψ (a shift to more negative, or less positive, values) when **1** is converted to **3**.

The results of 1-μs aqueous MD simulations of $\mathbf{1}^c$ and $\mathbf{3}^c$ are shown in Figures 5 and 6 and are summarized in Table 4. In $\mathbf{1}^c$

Table 4. Behavior of ϕ and ψ in $\mathbf{1}^c$ and $\mathbf{3}^c$ Determined from 1-μs Aqueous Molecular Dynamics Simulations

cmpd/states	parameter				
	population (%)	φ mean (°)	φ CSD[a] (°)	ψ mean (°)	ψ CSD (°)
$\mathbf{1}^c$					
state I	93.8	45.5	11.6	−1.1	18.1
state II	3.2	−25.3	16.8	−27.3	10.9
state III	3.0	45.0	15.7	−171.1	13.6
$\mathbf{3}^c$					
state I	71.6	40.5	11.6	−5.5	23.0
state II	11.2	−31.6	17.3	−30.0	13.9
state III	14.4	36.9	12.8	176.7	10.7
state IV	2.8	−179.8	10.0	−4.4	10.5

[a]CSD = circular standard deviation.

and $\mathbf{3}^c$, the dominant linkage conformations (94% for $\mathbf{1}^c$, 72% for $\mathbf{3}^c$) resemble those observed in the *MA'AT* models (Figure 5), with ϕ values of 46/41° and ψ values of −1.1°/−5.5°. While the absolute values differ from those obtained from *MA'AT* analysis, the trends in these angles are similar in that ϕ becomes less positive and ψ more negative upon C3 deoxygenation. Thus, the conclusion drawn from *MA'AT* modeling of ϕ and ψ in **1** and **3** with respect to the importance of inter-residue hydrogen bonding in dictating preferred linkage conformation is supported by the MD results.

Further inspection of the MD data reveals the presence of minor conformational states for the *O*-glycosidic linkages in $\mathbf{1}^c$ (states II and III) and $\mathbf{3}^c$ (states II–IV) (Table 4, Figures 5 and 6), and that their total population increases upon C3 deoxygenation (~6 to ~28%) (Table 4). 3D Structural representations of these states are shown in Figures S11 and S12 (Supporting Information). *MA'AT* analysis is not able to detect these minor states due to their low abundances and the limited number of experimental constraints used in the analyses, but it is noteworthy that rmsds calculated for single-state *MA'AT* models of ϕ and ψ in **1** and **3** are small (0.1–0.4 Hz) (Tables 3 and S3, Supporting Information), indicating that minor states, if present, are not highly populated. If the MD models are correct qualitatively, however, the results indicate that deoxygenation at C3 of the Glc residue of **1** results in access to a larger fraction of ϕ/ψ conformational space in **3** than in **1**. In this respect (i.e., access to a greater number of distinctly different ϕ/ψ rotamers), the overall flexibility of the linkage is predicted by MD simulation to be greater in **3** than in **1**. C3 deoxygenation itself, however, does not alter the ϕ and ψ torsion angles of the (highly) preferred linkage conformation to any appreciable extent and its effect on the librational motions of these angles is small.

CONCLUSIONS

This investigation aimed to determine the extent to which inter-residue hydrogen bonding in methyl α-lactoside (**1**) influences its preferred *O*-glycosidic linkage conformation in aqueous solution. A new NMR method, *MA'AT* analysis,[19,20] was applied to make this determination since it has the requisite sensitivity to relatively small changes in the mean torsion angles of ϕ and ψ in *O*-glycosidic linkages and provides information on librational averaging about these mean angles. We found that deletion of the hydroxyl group attached to C3 of **1**, which has been implicated in inter-residue hydrogen bonding to O5′ of the adjacent βGal residue at least in the crystalline state,[17] does not affect preferred linkage geometry to any appreciable extent. This conclusion is based on a comparison of *MA'AT*-determined ϕ and ψ values in **1** and in the C3-deoxy analogue **3**. If inter-residue hydrogen bonding exists in aqueous solutions of **1** and is relatively persistent, it may stabilize the linkage (i.e., lower its total energy), but it does not dictate the preferred linkage torsion angles. This conclusion is consistent with arguments made by French and co-workers from computational (DFT) studies of xylobiose[15] and by Hünenberger and co-workers from MD simulations of β-(1→4)-linked disaccharides.[56]

Aqueous MD simulation over 1 μs indicates that conformational exchange between a highly preferred geometry (i.e., that identified by *MA'AT* analysis) and several higher-energy linkage conformers is greater in C3-deoxy disaccharide **3** than in C3-oxy disaccharide **1**. These minor conformations are too low in abundance to be detected by *MA'AT* analysis, and consequently, *MA'AT* analysis cannot validate this behavior experimentally. What is clear, however, is that, in aqueous solution, noncovalent (electrostatic) interactions between O3H (donor) and O5′ (acceptor) in **1**, if appreciable in strength, only reinforce a linkage conformation that is intrinsically preferred in the absence of this interaction.

ASSOCIATED CONTENT

Supporting Information

The Supporting Information is available free of charge at https://pubs.acs.org/doi/10.1021/acs.jpcb.3c07448.

Preparation of disaccharide **3**; ^{1}H and ^{13}C chemical shifts in **3**; ^{1}H−^{1}H NMR spin-coupling constants in **3**; 600 MHz ^{1}H NMR spectrum of **3**; 150 MHz ^{13}C{^{1}H} NMR spectrum of **3**; partial 150 MHz ^{13}C{^{1}H} NMR spectra of $\mathbf{3}^{1'}$ and $\mathbf{3}^{2'}$; partial 2D J-HMBC spectrum of **3** showing the measurement of the trans-*O*-glycosidic $^3J_{C1',H4}$; partial 2D J-HMBC spectrum of **3** showing the measurement of the trans-*O*-glycosidic $^3J_{C4,H1'}$; torsional constraints applied to $\mathbf{3}^c$ during DFT calculations; hypersurfaces for ϕ-dependent *J*-couplings in $\mathbf{1}^c$ and $\mathbf{3}^c$; hypersurfaces for ψ-dependent *J*-couplings in $\mathbf{1}^c$ and $\mathbf{3}^c$; plots of six trans-*O*-glycosidic *J*-couplings calculated by DFT in $\mathbf{3}^c$, showing all data points; parameterized equations for trans-*O*-glycosidic spin-couplings in $\mathbf{1}^c$ and $\mathbf{3}^c$; parameter space plots for single-state *MA'AT* models of ϕ and ψ in **1** and **3**; DFT-determined potential energy surfaces for $\mathbf{1}^c$ and $\mathbf{3}^c$; experimental and back-calculated trans-*O*-glycosidic spin-couplings in **1** and **3**; representative 3D structures extracted from a 1-μs aqueous MD simulation of $\mathbf{1}^c$; representative 3D structures extracted from a 1-μs aqueous MD simulation of $\mathbf{3}^c$; and Cartesian coordinates for select conformers of $\mathbf{1}^c$ and $\mathbf{3}^c$; complete references 35, 48 and 54 (PDF)

AUTHOR INFORMATION

Corresponding Author

Anthony S. Serianni − *Department of Chemistry and Biochemistry, University of Notre Dame, Notre Dame,*

https://doi.org/10.1021/acs.jpcb.3c07448
J. Phys. Chem. B 2024, 128, 2317−2325

Indiana 46556, United States; orcid.org/0000-0001-6114-1446; Email: aseriann@nd.edu

Authors

Wenhui Zhang − *Department of Chemistry and Biochemistry, University of Notre Dame, Notre Dame, Indiana 46556, United States;* orcid.org/0000-0003-0089-0931

Reagan J. Meredith − *Department of Chemistry and Biochemistry, University of Notre Dame, Notre Dame, Indiana 46556, United States;* orcid.org/0000-0001-7330-3190

Xiaocong Wang − *Hubei Key Laboratory of Agricultural Bioinformatics, College of Informatics, Huazhong Agricultural University, Wuhan, Hubei 430070, China;* orcid.org/0000-0002-5387-7389

Robert J. Woods − *Complex Carbohydrate Research Center, University of Georgia, Athens, Georgia 30602, United States;* orcid.org/0000-0002-2400-6293

Ian Carmichael − *Radiation Laboratory, University of Notre Dame, Notre Dame, Indiana 46556, United States*

Complete contact information is available at: https://pubs.acs.org/10.1021/acs.jpcb.3c07448

Notes

The authors declare no competing financial interest.

■ ACKNOWLEDGMENTS

Financial support was provided by the National Science Foundation (CHE 1402744 and 1707660 to A.S.S.; CHE 2002628 to X.W. and R.J.W.) and by Omicron Biochemicals, Inc. The Notre Dame Radiation Laboratory is supported by the Department of Energy Office of Science, Office of Basic Energy Sciences under award number DE-FC02-04ER15533. This is document number NDRL 9272.

■ REFERENCES

(1) Pace, C. N.; Fu, H.; Lee Fryar, K.; Landua, J.; Trevino, S. R.; Schell, D.; Thurlkill, R. L.; Imura, S.; Scholtz, J. M.; Gajiwala, K.; Sevcik, J.; Urbanikova, L.; Myers, J. K.; Takano, K.; Hebert, E. J.; Shirley, B. A.; Grimsley, G. R. Contribution of Hydrogen Bonds to Protein Stability. *Protein Sci.* **2014**, *23*, 652−661.

(2) Goodman, M. F. Hydrogen Bonding Revisited: Geometric Selection as a Principal Determinant of DNA Replication Fidelity. *Proc. Natl. Acad. Sci. U.S.A.* **1997**, *94*, 10493−10495.

(3) Jeffrey, G. A. Intramolecular Hydrogen-Bonding In Carbohydrate Crystal-Structures. *Carbohydr. Res.* **1973**, *28*, 233−241.

(4) Kroon, J.; Kroon-Batenburg, L. M. J.; Leeflang, B. R.; Vliegenthart, J. F. G. Intramolecular Versus Intermolecular Hydrogen Bonding in Solution. *J. Mol. Struct.* **1994**, *322*, 27−31.

(5) Engelsen, S. B.; Monteiro, C.; Hervé de Penhoat, C.; Pérez, S. The Diluted Aqueous Solvation of Carbohydrates As Inferred From Molecular Dynamics Simulations and NMR Spectroscopy. *Biophys. Chem.* **2001**, *93*, 103−127.

(6) Corzana, F.; Motawia, M. S.; Hervé du Penhoat, C.; van den Berg, F.; Blennow, A.; Perez, S.; Engelsen, S. B. Hydration of the Amylopectin Branch Point. Evidence of Restricted Conformational Diversity of the α-(1→6) Linkage. *J. Am. Chem. Soc.* **2004**, *126*, 13144−13155.

(7) Almond, A. Towards Understanding the Interaction Between Oligosaccharides and Water Molecules. *Carbohydr. Res.* **2005**, *340*, 907−920.

(8) Hansen, P. I.; Larsen, F. H.; Motawia, S. M.; Blennow, A.; Spraul, M.; Dvortsak, P.; Engelsen, S. B. Structure and Hydration of the Amylopectin Trisaccharide Building Blocks − Synthesis, NMR, and Molecular Dynamics. *Biopolymers* **2008**, *89*, 1179−1193.

(9) Zhang, W.; Zhao, H.; Carmichael, I.; Serianni, A. S. An NMR Investigation of Putative Inter-residue H-Bonding in Methyl α-Cellobioside in Solution. *Carbohydr. Res.* **2009**, *344*, 1582−1587.

(10) Battistel, M. D.; Pendrill, R.; Widmalm, G.; Freedberg, D. I. Direct Evidence for Hydrogen Bonding in Glycans: A Combined NMR and Molecular Dynamics Study. *J. Phys. Chem. B.* **2013**, *117*, 4860−4869.

(11) Battistel, M. D.; Azurmendi, H. F.; Frank, M.; Freedberg, D. I. Uncovering Nonconventional and Conventional Hydrogen Bonds in Oligosaccharides Through NMR Experiments and Molecular Modeling: Application to Sialyl Lewis-X. *J. Am. Chem. Soc.* **2015**, *137*, 13444−13447.

(12) Battistel, M. D.; Azurmendi, H. F.; Freedberg, D. I. Glycan OH Exchange Rate Determination in Aqueous Solution: Seeking Evidence for Transient Hydrogen Bonds. *J. Phys. Chem. B.* **2017**, *121*, 683−695.

(13) Rönnols, J.; Engström, O.; Schnupf, U.; Säwén, E.; Brady, J. W.; Widmalm, G. Inter-Residual Hydrogen Bonding in Carbohydrates Unraveled by NMR Spectroscopy and Molecular Dynamics Simulations. *ChemBioChem* **2019**, *20*, 2519−2528.

(14) Hikiri, S.; Hayashi, T.; Ikeguchi, M.; Kinoshita, M. Statistical Thermodynamics For the Unexpectedly Large Difference Between Disaccharide Stereoisomers in Terms of Solubility in Water. *Phys. Chem. Chem. Phys.* **2018**, *20*, 23684−23693.

(15) Ling, Z.; Edwards, J. V.; Nam, S.; Xu, F.; French, A. D. Conformational Analysis of Xylobiose by DFT Quantum Mechanics. *Cellulose* **2020**, *27*, 1207−1224.

(16) Kwon, J.; Ruda, A.; Azurmendi, H. F.; Zarb, J.; Battistel, M. D.; Liao, L.; Asnani, A.; Auzanneau, F.-I.; Widmalm, G.; Freedberg, D. I. Glycan Stability and Flexibility: Thermodynamic and Kinetic Characterization of Nonconventional Hydrogen Bonding in Lewis Antigens. *J. Am. Chem. Soc.* **2023**, *145*, 10022−10034.

(17) Pan, Q.; Noll, B. C.; Serianni, A. S. Methyl 4-*O*-β-D-Galactopyranosyl-α-D-glucopyranoside (Methyl α-Lactoside). *Acta Crystallogr.* **2005**, *61*, o674−o677.

(18) Stenutz, R.; Shang, M.; Serianni, A. S. Methyl β-Lactoside (Methyl 4-*O*-β-D-Galactopyranosyl-β-D-glucopyranoside) Methanol Solvate. *Acta Crystallogr.* **1999**, *55*, 1719−1721.

(19) Meredith, R. J.; Sernau, L.; Serianni, A. S. *MA'AT*: A Web-Based Application to Determine Rotamer Population Distributions in Solution from Nuclear Magnetic Resonance Spin-Coupling Constants. *J. Chem. Inf. Model.* **2022**, *62*, 3135−3141.

(20) Meredith, R. J.; Carmichael, I.; Woods, R. J.; Serianni, A. S. *MA'AT* Analysis: Probability Distributions of Molecular Torsion Angles in Solution from NMR Spectroscopy. *Acc. Chem. Res.* **2023**, *56*, 2313−2328.

(21) Zhang, W.; Turney, T.; Meredith, R.; Pan, Q.; Sernau, L.; Wang, X.; Hu, X.; Woods, R. J.; Carmichael, I.; Serianni, A. S. Conformational Populations of β-(1→4) *O*-Glycosidic Linkages Using Redundant NMR *J*-Couplings and Circular Statistics. *J. Phys. Chem. B* **2017**, *121*, 3042−3058.

(22) Lemieux, R. Effects of unshared pairs of electrons and their solvation on conformational equilibria. *Pure Appl. Chem.* **1971**, *25*, 527−548.

(23) Praly, J.-P.; Lemieux, R. U. Influence of Solvent on the Magnitude of the Anomeric Effect. *Can. J. Chem.* **1987**, *65*, 213−223.

(24) Thøgersen, H.; Lemieux, R. U.; Bock, K.; Meyer, B. Further Justification for the *Exo*-anomeric Effect. Conformational Analysis Based on Nuclear Magnetic Resonance Spectroscopy of Oligosaccharides. *Can. J. Chem.* **1982**, *60*, 44−57.

(25) Kirby, A. J. *The Anomeric Effect and Related Stereoelectronic Effects at Oxygen*; Springer Verlag: Berlin, 1983.

(26) AlabuginStereoelectronic Effects, I. V. *A Bridge Between Structure and Reactivity*; John Wiley & Sons: West Sussex, U.K., 2016.

(27) Juaristi, E.; Cuevas, G. *The Anomeric Effect*; CRC Press: Boca Raton, 1995; pp 95−111.

(28) Bose, B.; Zhao, S.; Stenutz, R.; Cloran, F.; Bondo, P. B.; Bondo, G.; Hertz, B.; Carmichael, I.; Serianni, A. S. Three-Bond C−O−C−C Spin-Coupling Constants in Carbohydrates: Development of a Karplus Relationship. *J. Am. Chem. Soc.* **1998**, *120*, 11158−11173.

(29) Cloran, F.; Carmichael, I.; Serianni, A. S. Density Functional Calculations on Disaccharide Mimics: Studies of Molecular Geometries and Trans-*O*-Glycosidic $^{3}J_{COCH}$ and $^{3}J_{COCC}$ Spin-Couplings. *J. Am. Chem. Soc.* **1999**, *121*, 9843−9851.
(30) Cloran, F.; Carmichael, I.; Serianni, A. S. $^{2}J_{COC}$ Spin-Spin Coupling Constants Across Glycosidic Linkages Exhibit a Valence Bond-Angle Dependence. *J. Am. Chem. Soc.* **2000**, *122*, 396−397.
(31) Hayes, M. L.; Serianni, A. S.; Barker, R. Methyl β-Lactoside: 600-MHz ^{1}H- and 75-MHz ^{13}C-NMR Studies of ^{2}H- and ^{13}C-Enriched Compounds. *Carbohydr. Res.* **1982**, *100*, 87−101.
(32) Serianni, A. S.; Nunez, H. A.; Barker, R. Carbon-13-Enriched Carbohydrates. Preparation of Aldononitriles and Their Reduction with a Palladium Catalyst. *Carbohydr. Res.* **1979**, *72*, 71−78.
(33) Zhang, W.; Zhao, S.; Serianni, A. S. Labeling Monosaccharides With Stable Isotopes. *Methods Enzymol.* **2015**, *565*, 423−458.
(34) Meissner, A.; Sørensen, O. W. Measurement of J(H,H) and Long-range J(X,H) Coupling Constants in Small Molecules. Broadband XLOC and *J*-HMBC. *Magn. Reson. Chem.* **2001**, *39*, 49−52.
(35) Frisch, M. J.; Trucks, G. W.; Schlegel, H. B.; Scuseria, G. E.; Robb, M. A.; Cheeseman, J. R.; Scalmani, G.; Barone, V.; Mennucci, B.; Petersson, G. A.; et al. *Gaussian09*. Revision D; Gaussian Inc.: Pittsburgh, PA, 2009.
(36) Becke, A. D. Density-Functional Thermochemistry. III. The Role of Exact Exchange. *J. Chem. Phys.* **1993**, *98*, 5648−5652.
(37) Hehre, W. J.; Ditchfield, R.; Pople, J. A. Self-Consistent Molecular Orbital Methods. XII. Further Extensions of Gaussian-Type Basis Sets for Use in Molecular Orbital Studies of Organic Molecules. *J. Chem. Phys.* **1972**, *56*, 2257−2261.
(38) Cances, E.; Mennucci, B.; Tomasi, J. A New Integral Equation Formalism for the Polarizable Continuum Model: Theoretical Background and Applications to Isotropic and Anisotropic Dielectrics. *J. Chem. Phys.* **1997**, *107*, 3032−3041.
(39) Cammi, R.; Mennucci, B.; Tomasi, J. Fast Evaluation of Geometries and Properties of Excited Molecules in Solution: A Tamm-Dancoff Model with Application to 4- Dimethylaminobenzonitrile. *J. Phys. Chem. A.* **2000**, *104*, 5631−5637.
(40) Sychrovsky, V.; Grafenstein, J.; Cremer, D. Nuclear Magnetic Resonance Spin−Spin Coupling Constants from Coupled Perturbed Density Functional Theory. *J. Chem. Phys.* **2000**, *113*, 3530−3547.
(41) Helgaker, T.; Watson, M.; Handy, N. C. Analytical Calculation of Nuclear Magnetic Resonance Indirect Spin−Spin Coupling Constants at the Generalized Gradient Approximation and Hybrid Levels of Density-Functional Theory. *J. Chem. Phys.* **2000**, *113*, 9402−9409.
(42) Barone, V.; Peralta, J. E.; Contreras, R. H.; Snyder, J. P. DFT Calculation of NMR J_{FF} Spin−Spin Coupling Constants in Fluorinated Pyridines. *J. Chem. Phys.* **2002**, *106*, 5607−5612.
(43) Stenutz, R.; Carmichael, I.; Widmalm, G.; Serianni, A. S. Hydroxymethyl Group Conformation in Saccharides: Structural Dependencies of $^{2}J_{HH}$, $^{3}J_{HH}$ and $^{1}J_{CH}$ Spin-Spin Coupling Constants. *J. Org. Chem.* **2002**, *67*, 949−958.
(44) Zhang, W.; Meredith, R.; Pan, Q.; Wang, X.; Woods, R. J.; Carmichael, I.; Serianni, A. S. Use of Circular Statistics To Model αMan-(1→2)-αMan and αMan-(1→3)-α/βMan *O*-Glycosidic Linkage Conformation in ^{13}C-Labeled Disaccharides and High-Mannose Oligosaccharides. *Biochemistry* **2019**, *58*, 546−560.
(45) Complex Carbohydrate Research Center (CRCC); University of Georgia. http://www.glycam.org (accessed Jan 17, 2024).
(46) Kirschner, K. N.; Yongye, A. B.; Tschampel, S. M.; González-Outeiriño, J.; Daniels, C. R.; Foley, B. L.; Woods, R. J. GLYCAM06: A Generalizable Biomolecular Force Field. Carbohydrates. *J. Comput. Chem.* **2008**, *29*, 622−655.
(47) Jorgensen, W. L.; Chandrasekhar, J.; Madura, J. D.; Impey, R. W.; Klein, M. L. Comparison of Simple Potential Functions for Simulating Liquid Water. *J. Chem. Phys.* **1983**, *79*, 926−935.
(48) Case, D. A.; Babin, V.; Berryman, J. T.; Betz, R. M.; Cai, Q.; Cerutti, D. S.; Cheatham, T. E. I.; Darden, T. A.; Duke, R. E.; Gohlke, H.; et al. *AMBER 14*; University of California: San Francisco, 2014.
(49) Berendsen, H. J. C.; Postma, J. P. M.; van Gunsteren, W. F.; DiNola, A.; Haak, J. R. Molecular Dynamics with Coupling to an External Bath. *J. Chem. Phys.* **1984**, *81*, 3684−3690.
(50) van Gunsteren, W. F.; Berendsen, H. J. C. Algorithms for Macromolecular Dynamics and Constraint Dynamics. *Mol. Phys.* **1977**, *34*, 1311−1327.
(51) Götz, A. W.; Williamson, M. J.; Xu, D.; Poole, D.; Le Grand, S.; Walker, R. C. Routine Microsecond Molecular Dynamics Simulations with AMBER on GPUs. 1. Generalized Born. *J. Chem. Theory Comput.* **2012**, *8*, 1542−1555.
(52) Kirschner, K. N.; Woods, R. J. Solvent Interactions Determine Carbohydrate Conformation. *Proc. Natl. Acad. Sci. U.S.A.* **2001**, *98*, 10541−10545.
(53) *Prism 8 for Mac OS X*; GraphPad Software, Version 8.4.2 (464), April 18, 2020.
(54) Hadad, M. J.; Zhang, W.; Turney, T.; Sernau, L.; Wang, X.; Woods, R. J.; Incandela, A.; Surjancev, I.; Wang, A.; Yoon, M.-K.; et al. NMR Spin-Couplings in Saccharides: Relationships Between Structure, Conformation and the Magnitudes of J_{HH}, J_{CH} and J_{CC} Values. In *New Developments in NMR 10: NMR in Glycoscience and Glycotechnology*; Peters, T., Kato, K., Eds.; Royal Society of Chemistry, 2017; pp 20−100.
(55) Meredith, R. J.; Carmichael, I.; Serianni, A. S. Nonconventional NMR Spin-Coupling Constants in Oligosaccharide Conformational Modeling: Structural Dependencies Determined from Density Functional Theory Calculations. *ACS Omega* **2022**, *7*, 23950−23966.
(56) Wang, D.; Ámundadóttir, M. L.; van Gunsteren, W. F.; Hünenberger, P. H. Intramolecular hydrogen-bonding in aqueous carbohydrates as a cause or consequence of conformational preferences: a molecular dynamics study of cellobiose stereoisomers. *Eur. Biophys. J.* **2013**, *42*, 521−537.

https://doi.org/10.1021/acs.jpcb.3c07448
J. Phys. Chem. B 2024, 128, 2317−2325